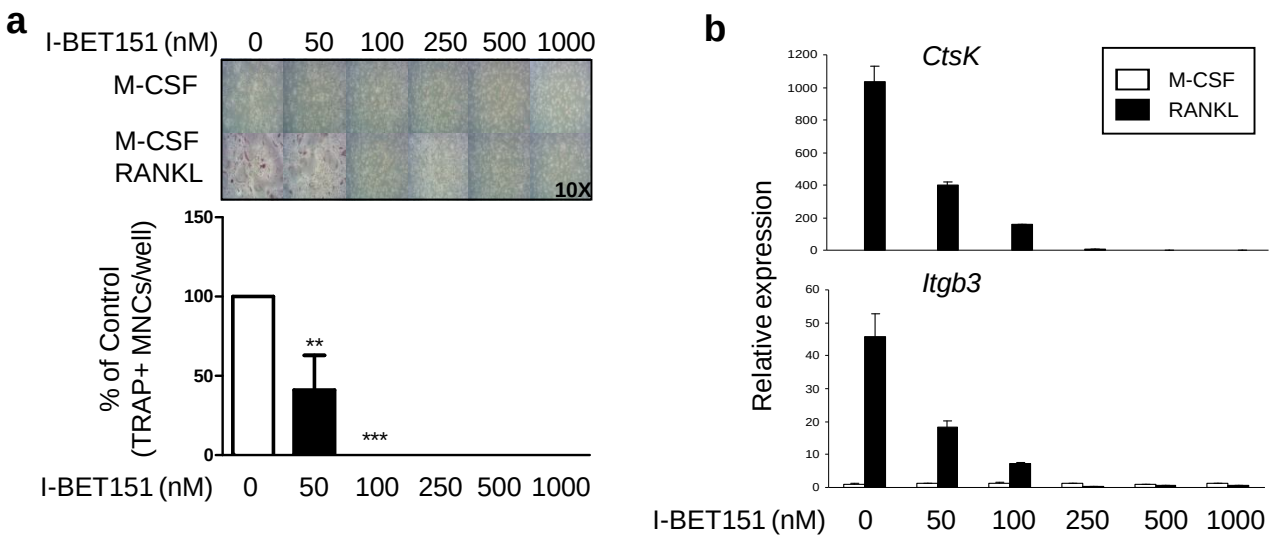

Supplementary Figure 1. I-BET151 inhibits murine osteoclastogenesis. a. Mouse bone marrow cells from C57BL/6 mice were cultured with M-CSF (20 ng ml^{-1}) for 4 days and then exposed to either DMSO (vehicle control, labeled 0) or I-BET151 at the indicated doses. After 1hr, RANKL (100 ng ml^{-1}) was added, and TRAP-positive multinucleated (more than three nuclei) cells were counted 5 days after RANKL addition. The number of osteoclasts in control conditions is set as 100%. *Upper panel*, Representative results obtained from one out of more than three experiments are shown. *Lower panel,* Data are shown as means ± SEM from three independent experiments. ** :$P < 0.01$, *** :$P < 0.001$ by One-way ANOVA. **b.** Cells were cultured as in **a,** and mRNA was measured using real-time PCR. mRNA levels were normalized relative to the expression of GAPDH mRNA. Representative results from at least three independent experiments are shown.

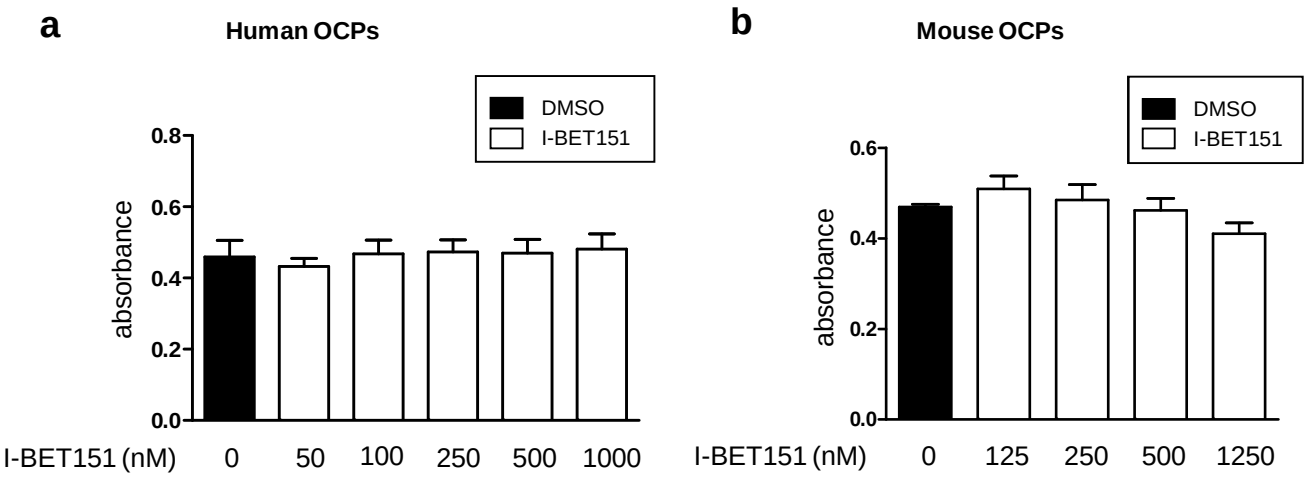

Supplementary Figure 2. Effect of I-BET151 on cell survival. Either human OCPs (**a**, CD14+ monocytes cultured overnight with M-CSF (20 ng ml^{-1})) or mouse OCPs (**b**, bone marrow cells cultured with M-CSF for four days) were cultured with either DMSO (black bars) or I-BET151 (white bars) at the indicated doses for six days and then cell viability was measured using the MTT assay kit (Roche). Absorbances (A590-A690) are shown as means ± SEM from four independent experiments with human OCPs and five independent experiments with mouse OCPs.

Supplementary Figure 3

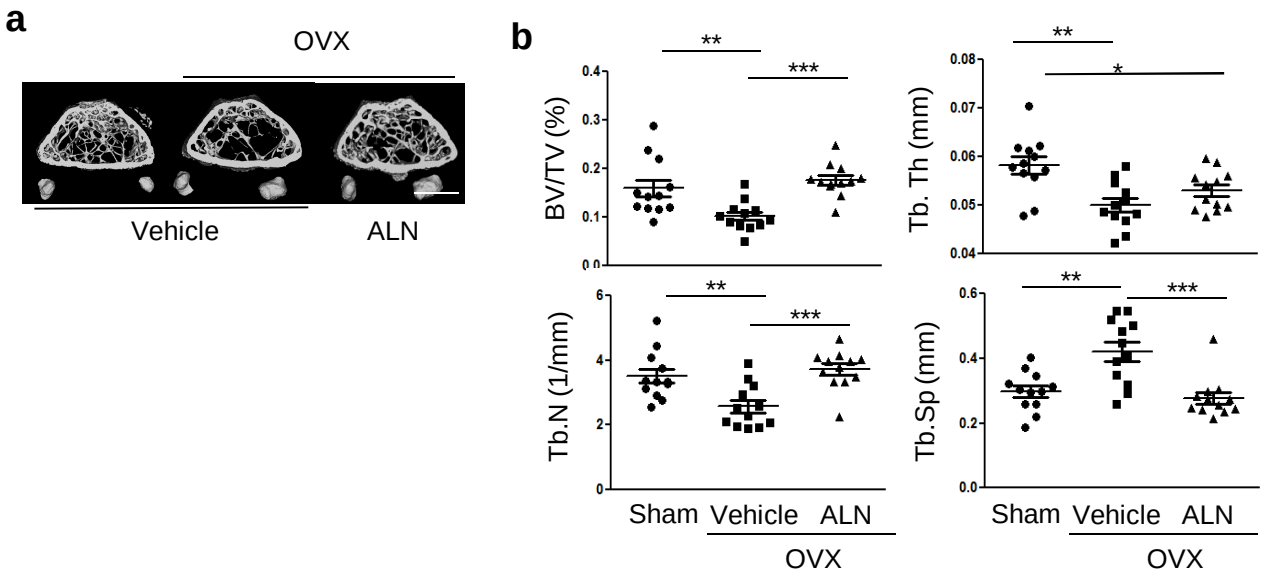

Supplementary Figure 3. Alendronate increases bone mass in the post-OVX model of osteoporosis. The effects of alendronate (ALN, n=12) in the OVX-induced bone loss model were tested in parallel to the effects of I-BET151 in the same experiment as shown in Fig. 2; thus, the control data for sham-operated mice (Sham) and ovariectomized mice (OVX) are the same in Fig. 2 and Supplementary Figure 3. **a.** Representative images showing trabecular architecture by micro-computed tomography (μCT) reconstruction in the distal femurs. Scale bars, 1 mm. **b.** μCT measurements for the indicated parameters in distal femurs. Bone volume (BV TV^{-1}), trabecular space (Tb.Sp.), trabecular number (Tb.N.) and trabecular thickness (Tb.Th.) were determined by μCT analysis. All data are shown as mean ± SEM * P<0.05, ** P <0.01, *** P <0.001. One-way ANOVA with a posthoc Tukey test was performed.

Supplementary Figure 4

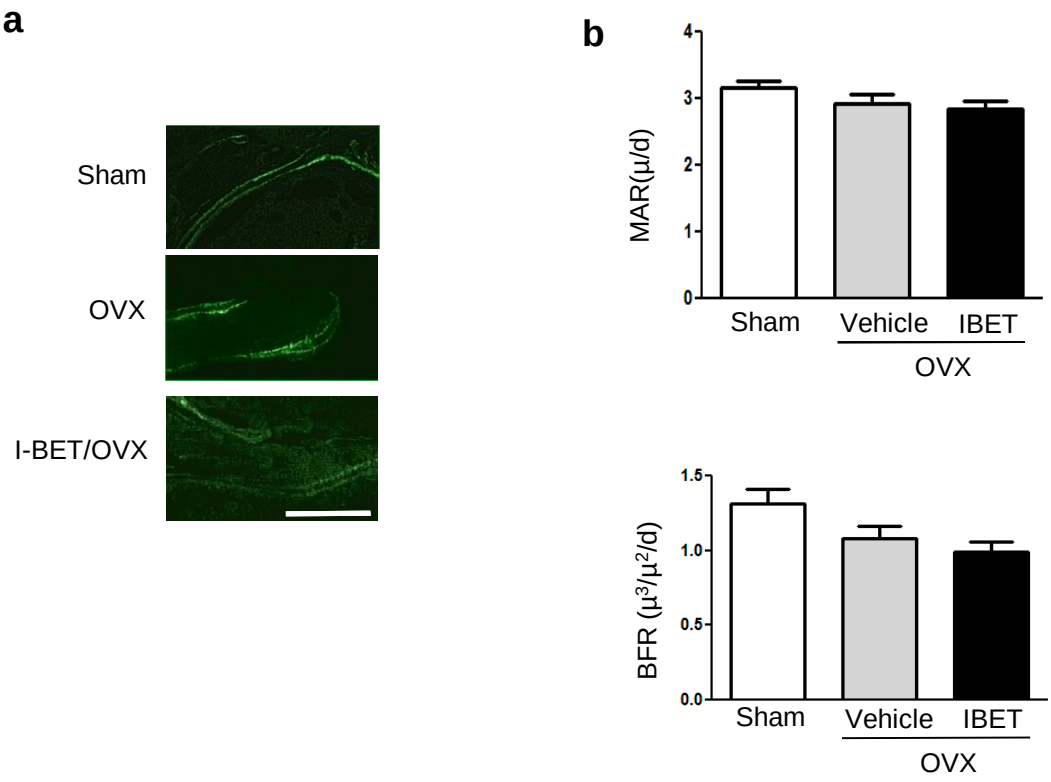

Supplementary Figure 4. I-BET151 did not significantly suppress bone formation in the post-ovariectomy model. a. Representative images showing casein double labeling in trabecular bone. Scale bars 100 μm. **b.** Bone formation parameters including mineral apposition rate (MAR) and bone formation rate (BFR) were measured in sham-operated mice (Sham), ovariectomized mice (OVX) and I-BET 151 treated group (IBET/OVX) (n=6). All data are shown as mean ± SEM and the statistical analysis (One-way ANOVA) showed no significant difference among groups.

a

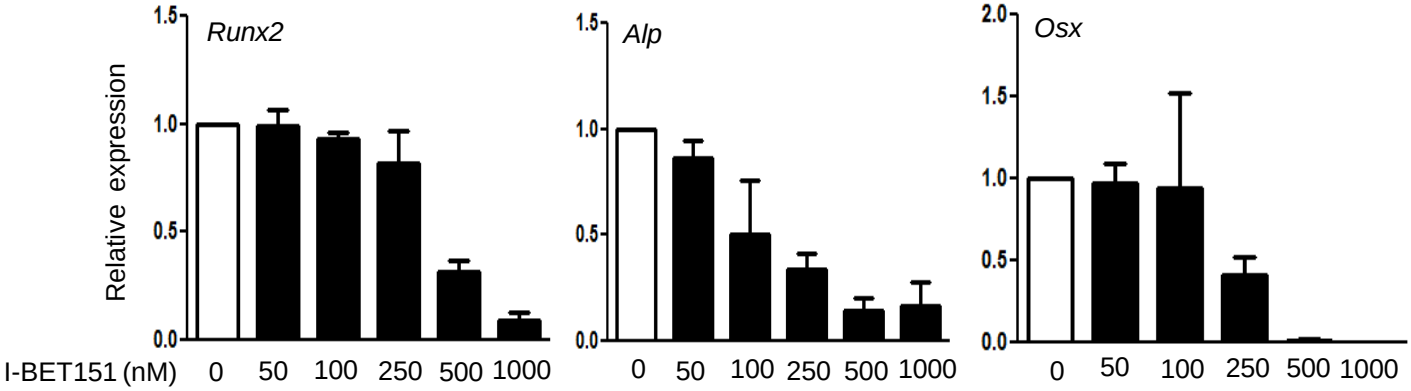

b

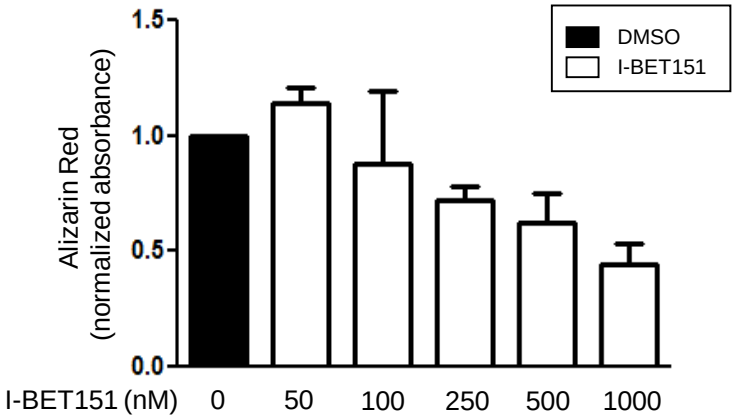

Supplementary Figure 5. The dose-dependent effect of I-BET151 on osteoblast cultures. Primary osteoblasts were isolated from calvariae and cultured with α-MEM containing 10% FBS, 50 μg $ml^{-1}$of ascorbic acid, and 8 mM beta-glycerophosphate. Cells were treated with either DMSO or I-BET151 at the indicated doses from the beginning of the culture. **a.** mRNA was measured using real-time PCR at day 10. mRNA levels were normalized relative to the expression of GAPDH and results are shown as mean ± SEM from two independent experiments. **b.** Alizarin Red Staining of mineralizing osteoblast cells. Values were normalized relative to control cells treated with vehicle control DMSO. All data are shown as mean ± SEM from two independent experiments.

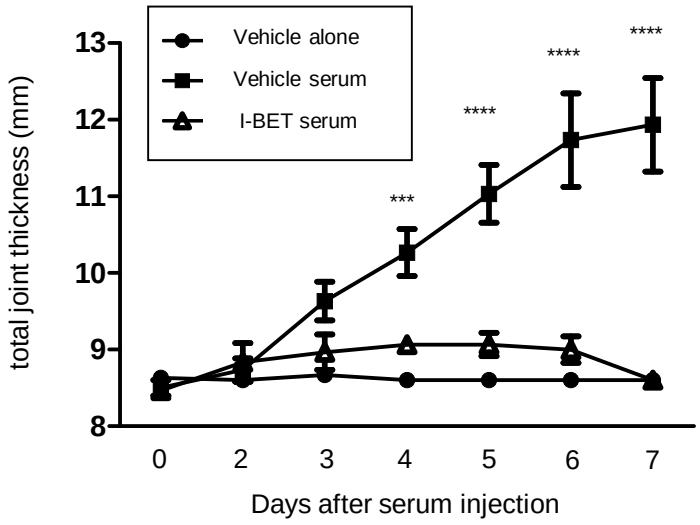

Supplementary Figure 6. I-BET151 nearly completely suppresses K/BxN arthritis induced by suboptimal amounts of serum. Arthritis was induced in C57BL/6 mice as described in Methods, except that a low potency arthritogenic serum was used. Under these conditions, where arthritis in the control serum-treated group was milder than that shown in Fig. 3, only minimal arthritis occurred in the I-BET151-treated group. Shown is the time course of arthritis development in the presence and absence of I-BET151 treatment. Values are the mean ± SEM of 3 mice per group. *** :$P < 0.001$; ****: $P < 0.0001$ by two-way ANOVA.

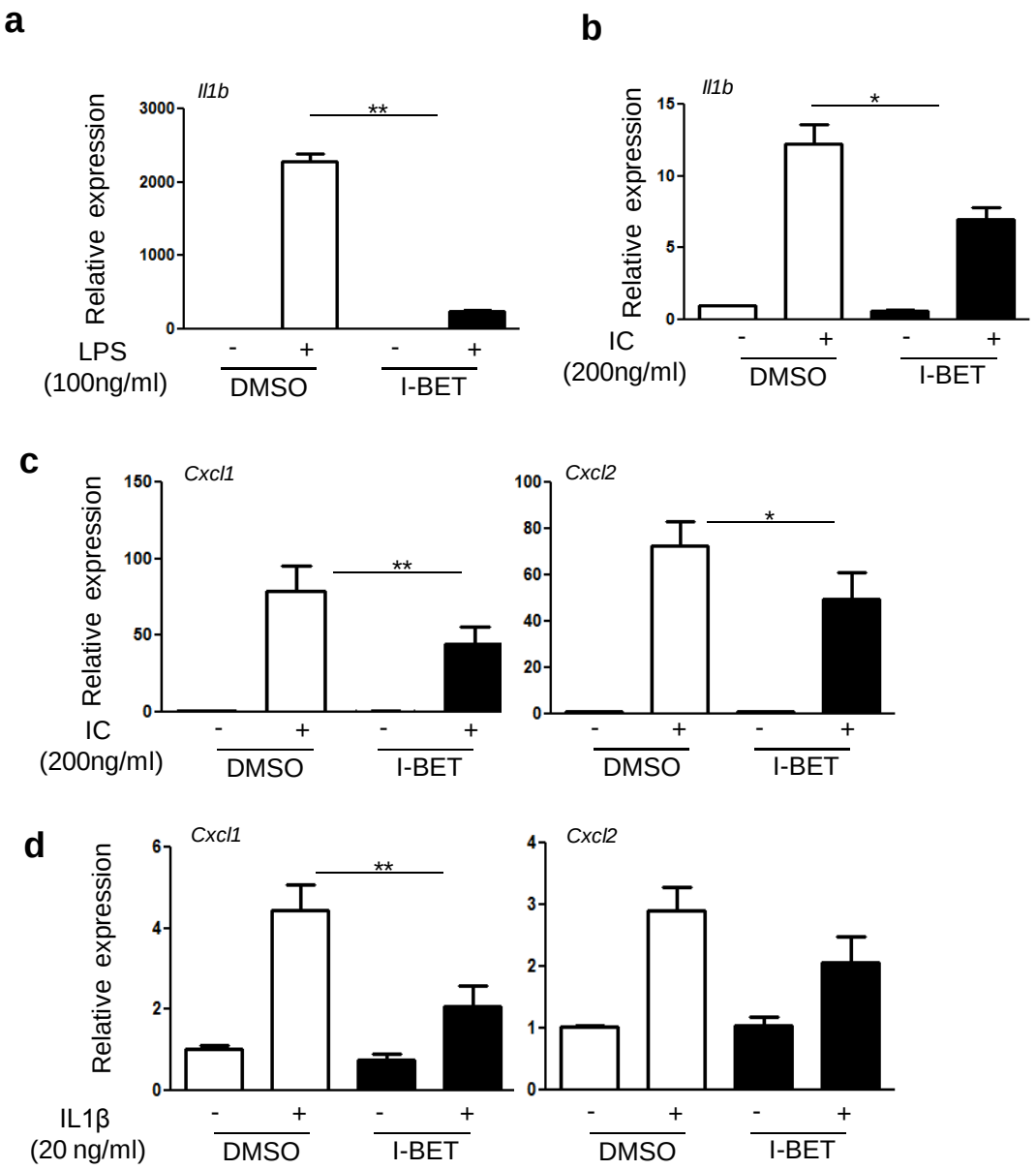

Supplementary Figure 7. I-BET151 suppresses induction of IL-1 by inflammatory stimuli and attenuates immune complex- and IL-1-induced expression of neutrophil chemoattractants. Mouse OCPs were treated with DMSO or I-BET151 (500 nM) for 1hr prior to stimulation with inflammatory stimuli. **a.** Cells were stimulated with LPS (**a**, 100 ng ml^{-1}) for 6 hrs. **b-d**. Cells were stimulated with immune complexes (IC; 200 ng ml^{-1}) that were formed by incubation of anti-DNP with DNP-albumin (**b, c**), or murine IL-1β (**d**, 20 ng/ml) for 3 hrs. mRNA was measured using real-time PCR. mRNA levels were normalized to the expression of GAPDH, and results are shown as means ± SEM from three experiments. * :$P < 0.05$, ** :$P < 0.01$ by *t*-test.

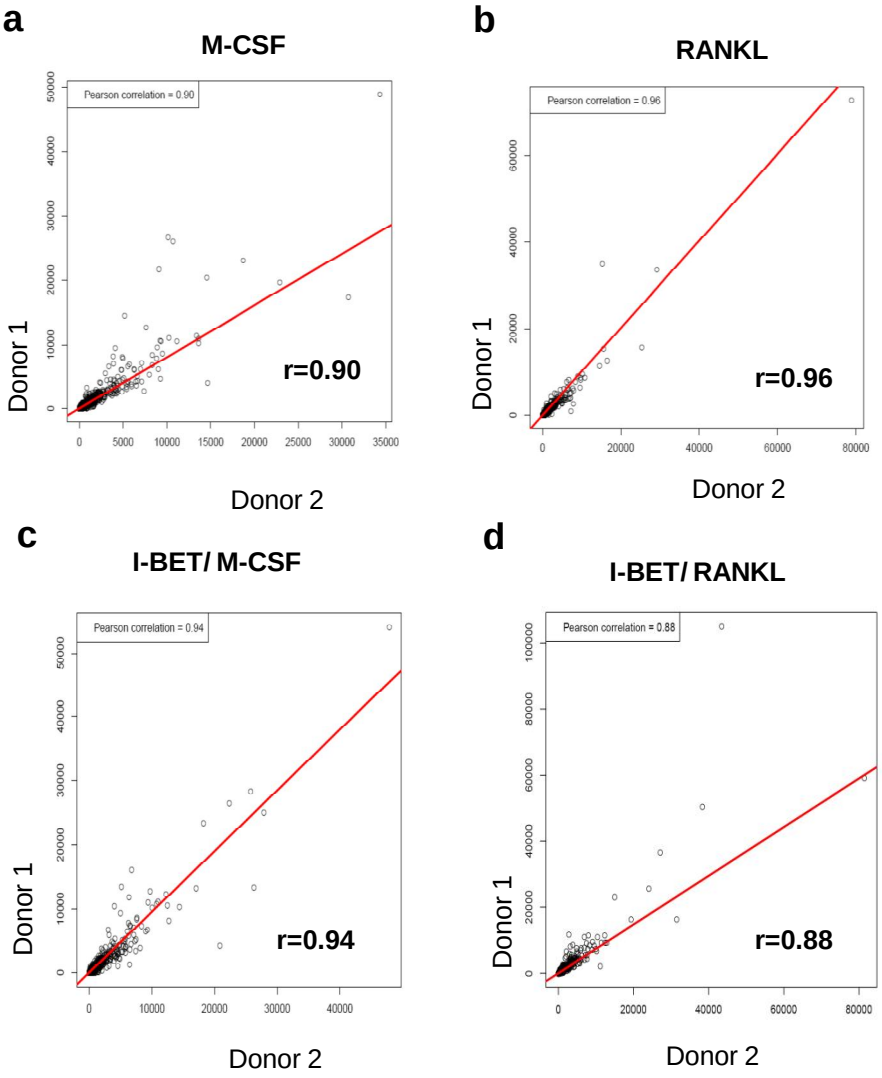

Supplementary Figure 8. Pearson correlation analysis of RNAseq data obtained using OCPs from two independent donors. Human OCPs (CD14+ monocytes cultured overnight with M-CSF (20 ng ml^{-1})) were treated with DMSO (vehicle control, labeled 0) or I-BET151 (250nM) for 1hr prior to addition of RANKL (40 ng ml^{-1}). Cells were incubated with RANKL for one day. **a-d,** The scatter plot diagrams show Pearson correlation analysis of gene expression profiles of human OCPs between two independent donors. The red lines in the scatter plots show the linear model trend line of the data. The first donor is plotted on the Y-axis and the second donor on the X-axis. The respective correlation coefficient values are reported in each plot. Pearson correlation coefficients were > 0.88, showing similarity of gene expression in biological replicates.

a **Molecular and Cellular Function**

Name	p-value	# of molecules
Cell Cycle	1.58E-22 - 3.54E-0.3	118
Cellular Assembly and Organization	7.43E-19 - 3.05E-03	107
DNA Replication, Recombination, Repair	7.43E-19 - 3.21E-03	111
Cellular Development	2.61E-11 - 3.41E-0.3	110
Cellular Growth and Proliferation	2.61E-11 - 3.14E-03	154

b **Top canonical pathway**

Name	p-value	Ratio
Estrogen-mediated S-phase Entry	1.54E-09	0.321
Cell Cycle Control of Chromosomal Replication	7.48E-09	0.265
Cyclins and Cell Cycle Regulation	3.1E-08	0.135
Mitotic Roles of Polo-like Kinase	3.24E-07	0.149
Role of CHK Proteins in Cell Cycle Checkpoint Control	4.16E-07	0.169

Supplementary Figure 9. Analysis of RNAseq data: Gene ontology (GO) analysis of 465 RANKL-induced genes which I-BET151 suppressed by > 50% in two independent donors. To gain insight into mechanisms by which I-BET151 suppressed osteoclastogenesis, we analyzed RANKL-induced genes whose expression was inhibited >50% by I-BET151 (in other words, I-BET151 targets) (listed in Supplementary Table 1). Visual inspection of the I-BET target gene list was followed by pathway and gene ontogeny (GO) analysis using Ingenuity Pathway Analysis (IPA, Ingenuity Systems, Redwood City, CA) and also the Molecular Signature Database available at the Broad Institute website www.broadinstitute.org/gsea. Consistent with the 24 hr time point of RANKL stimulation, which is early during the 5-6 day osteoclast differentiation process and precedes expression of many canonical osteoclast marker genes, osteoclast-related genes were not enriched among the I-BET targets (as these genes were not yet expressed in response to RANKL stimulation). In accordance with results shown in Supplemental Fig. 13, genes encoding components of osteoclast inducing pathways such as NF-kB or MAPK-AP-1 were not enriched. In contrast, GO analysis of molecular cellular function (**a**) and canonical pathways (**b**) using IPA showed highly significant enrichment of genes important in fundamental cellular processes such as cell cycle regulation, cell proliferation, and DNA replication and repair. GO analysis using the Molecular Signatures Database showed similar results (data not shown). These results are consistent with the known functions in cell cycle and proliferation of MYC and its inhibition by I-BET151, although the role of MYC and cell cycle regulators in these post-mitotic nonproliferating human OCPs needs to be further clarified.

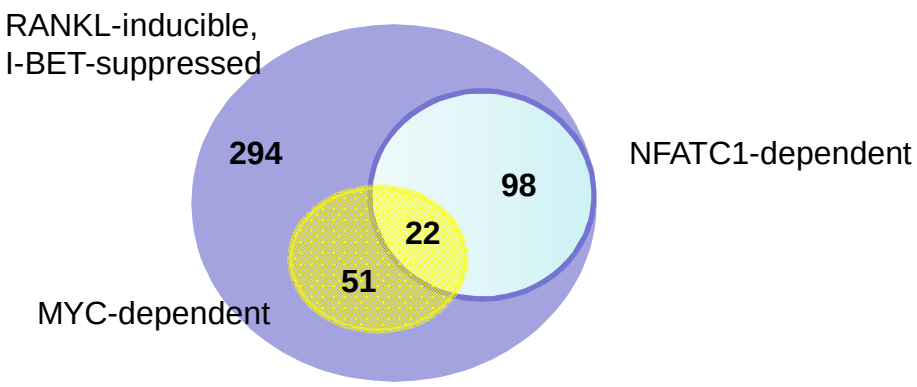

Supplementary Figure 10. Transcriptome-wide analysis reveals that I-BET151 suppresses RANKL-induced expression of MYC and NFAT target genes. We extended our analysis to ask whether the 465 I-BET targets were enriched in genes that are regulated by transcription factors important for osteoclastogenesis. Strikingly, 120 of 465 (26%) of I-BET targets correspond to NFATc1 target genes (GSE37219) [2] (shaded light blue in Venn diagram, listed in Supplementary Table 2). IPA analysis showed that 73 out of 465 (16%) of I-BET targets correspond to MYC target genes (shaded yellow in Venn diagram), which corroborates the results shown above. These results confirm that I-BET inhibits MYC in OCPs, and suggest that a major effect of I-BET is suppression of NFATc1 and expression of its target genes that play a key role in osteoclastogenesis.

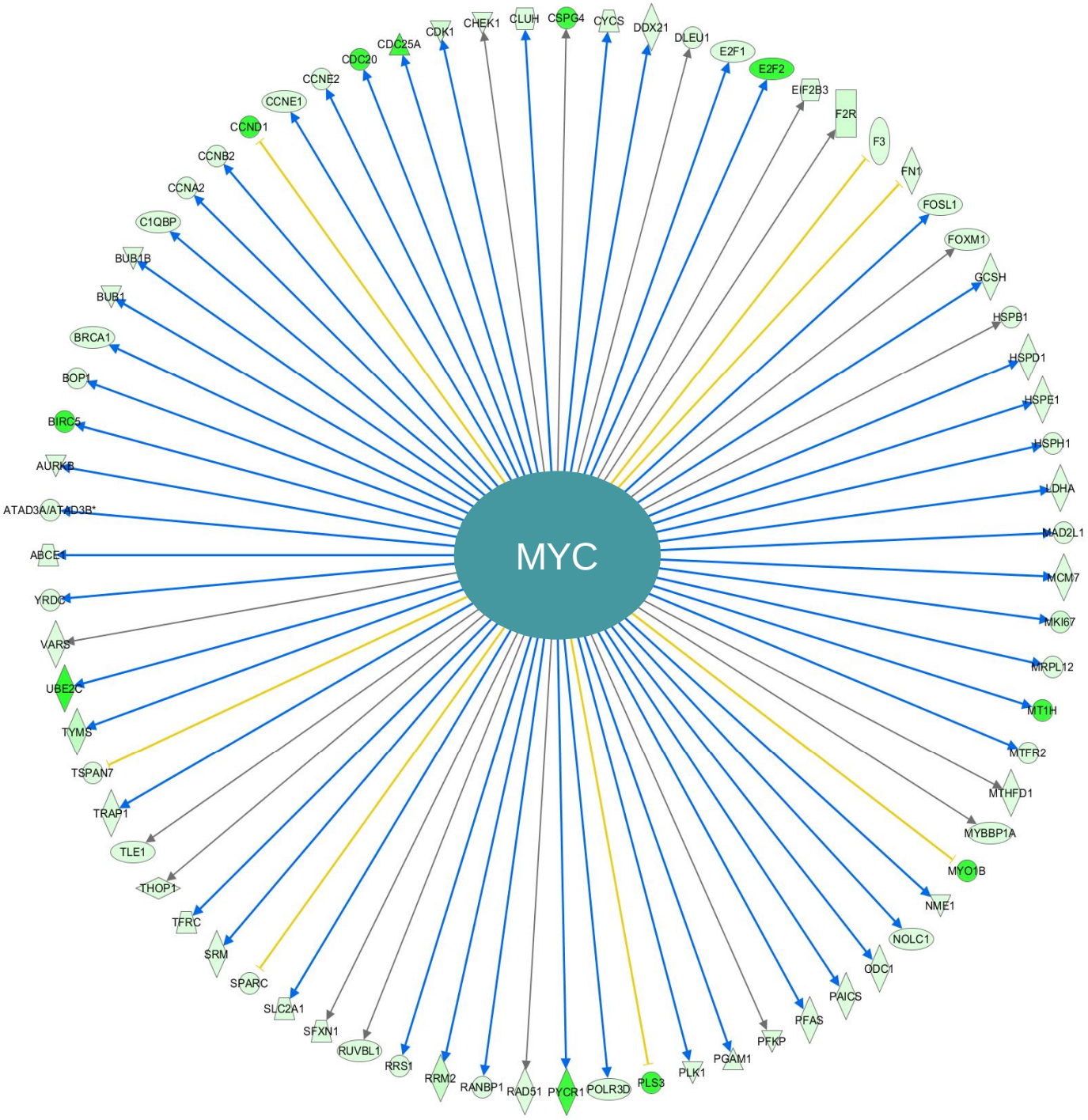

Supplementary Figure 11. MYC target gene network suppressed by I-BET151 in RANKL-stimulated OCPs. Results of IPA upstream regulator analysis that identified MYC as a regulator of I-BET151 targets are shown. Dark green: genes highly suppressed by IBET151; light green: genes less suppressed by IBET151. The arrows depict predicted relationships of MYC and target genes: blue arrows denote genes induced by MYC and yellow arrows denote genes regulated by MYC in a context-dependent manner.

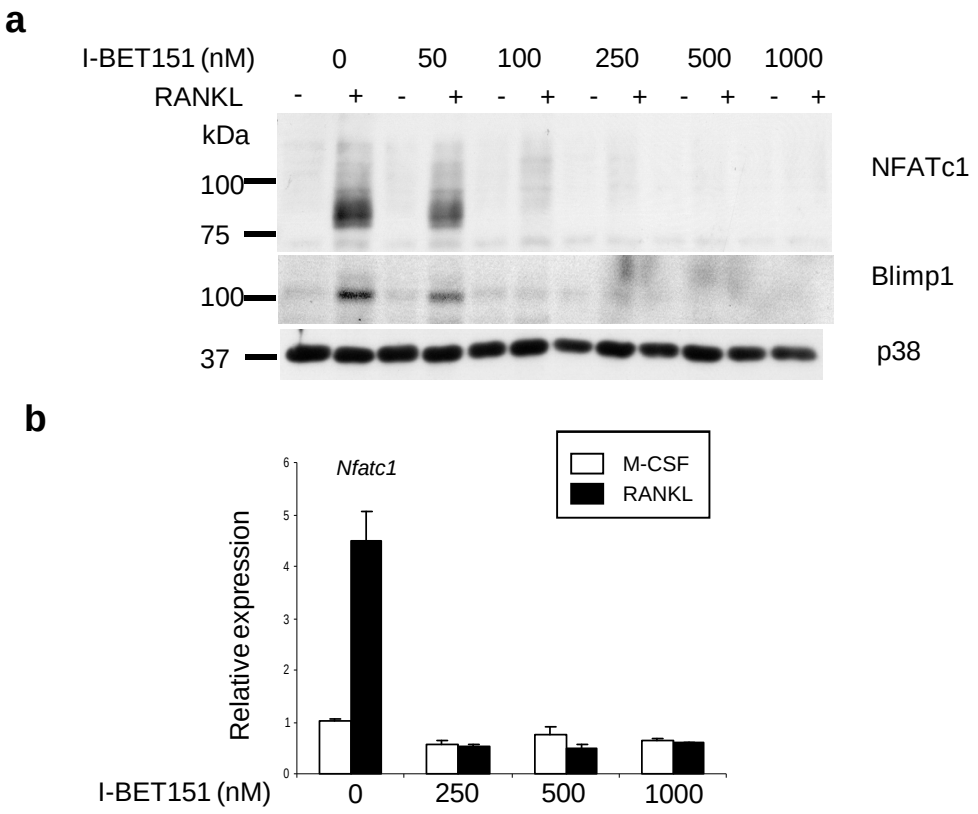

Supplementary Figure 12. I-BET151 suppresses RANKL-induced NFATc1 expression in mouse OCPs. Mouse bone marrow cells from C57BL/6 mice were cultured with M-CSF (20 ng ml^{-1}) for 4 days and then exposed to either DMSO (vehicle control, labeled 0) or I-BET151 at the indicated doses. After 1hr, RANKL (100 ng ml^{-1}) was added and cells were cultured with RANKL for two additional days. **a.** Whole-cell lysates were immunoblotted with NFATc1, Blimp1 and p38 antibodies. Images have been cropped for presentation; full size blots are shown in Supplementary Figure 18. **b.** mRNA was measured using real-time PCR. mRNA levels were normalized to the expression of GAPDH, and results are shown as means ± SD of triplicate determinants. The results are from more than three experiments.

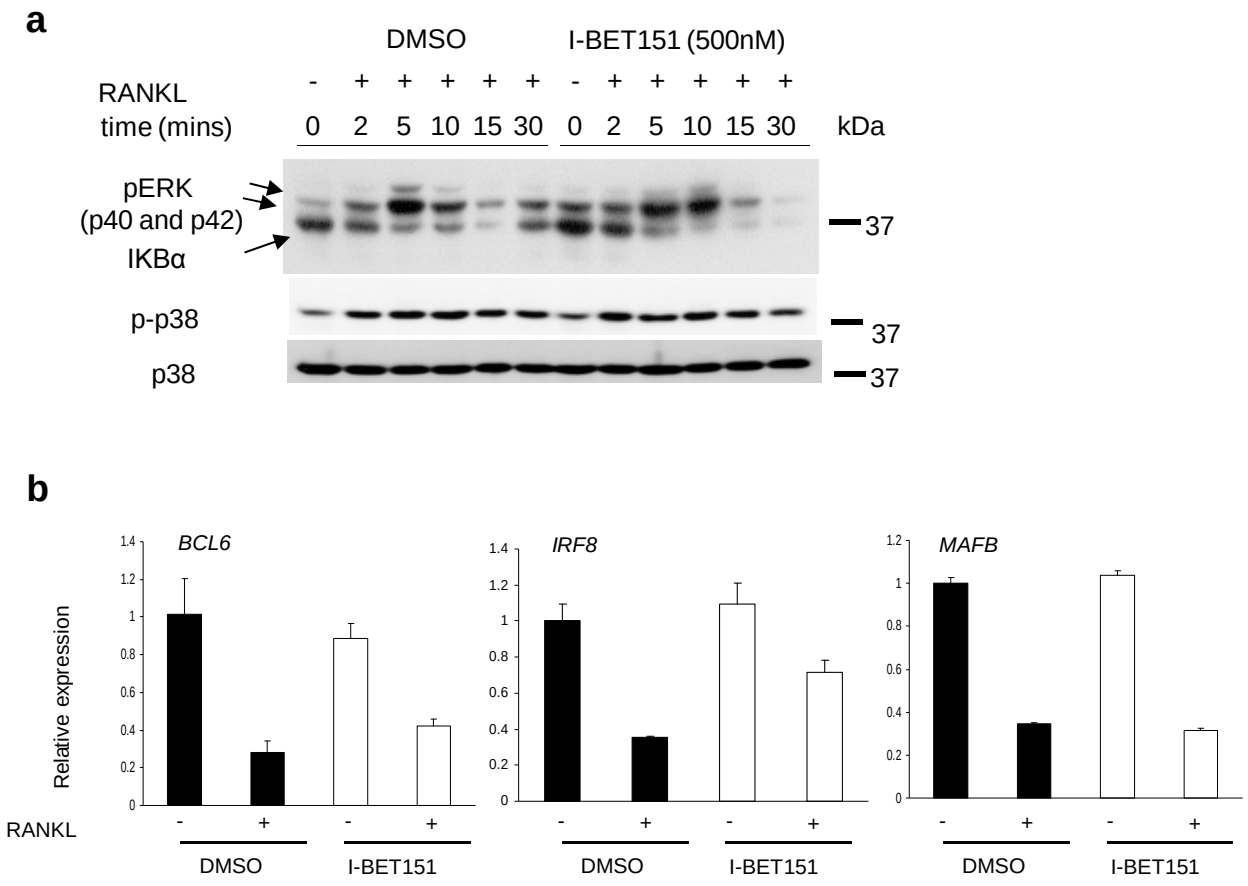

Supplementary Figure 13. I-BET151 minimally regulates proximal RANKL signaling pathways and RANKL-induced suppression of transcriptional repressors. Human OCPs were generated and then cultured in the presence or absence of I-BET151 (500nM) for 1 hr. **a.** OCPs were then stimulated with RANKL (100 ng ml^{-1}) for the indicated times. Whole-cell lysates were subjected to immunoblotting with the indicated antibodies. Images have been cropped for presentation; full size blots are shown in Supplementary Figure 18. **b.** OCPs were cultured with RANKL (40 ng ml^{-1}) for two additional days. mRNA levels of known repressors of osteoclastogenesis, BCL6, IRF8, and MAF-B, were measured using real-time PCR. RANKL stimulation resulted in the expected decreases in BCL6, IRF8 and MAF-B mRNA level. These decreases were not effectively reversed by I-BET151, suggesting that I-BET151 does not work by increasing expression of negative regulators of osteoclastogenesis. mRNA levels were normalized to the expression of GAPDH mRNA, and results are shown as means ± SD of triplicate determinants.

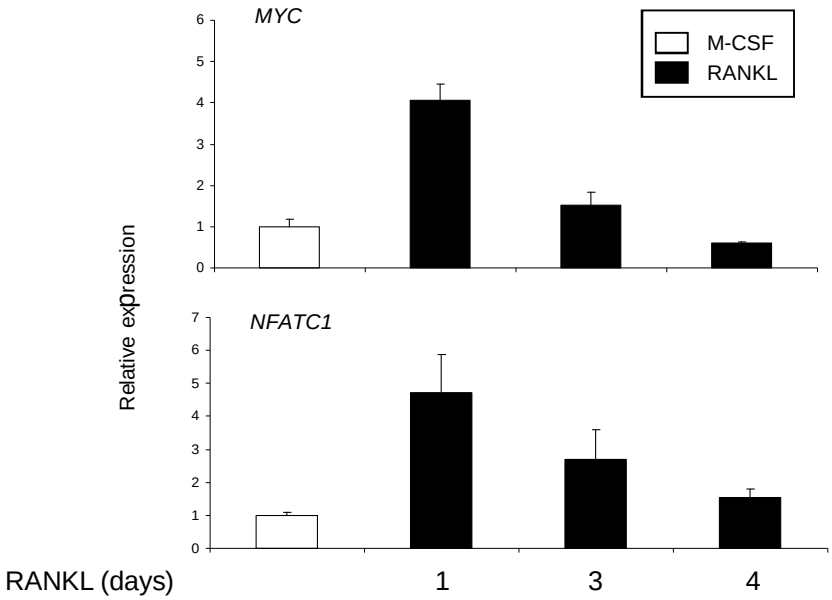

Supplementary Figure 14. Time course analysis of *MYC* and *NFATC1* expression in human OCPs. Human monocytes were cultured with M-CSF (20 ng ml^{-1}) for 1 day, and RANKL (40 ng ml^{-1}) was then added for the indicated times. mRNA was measured using real-time PCR. mRNA levels were normalized to the expression of GAPDH mRNA, and results are shown as means ± SD of triplicate determinants.

Mouse OCPs

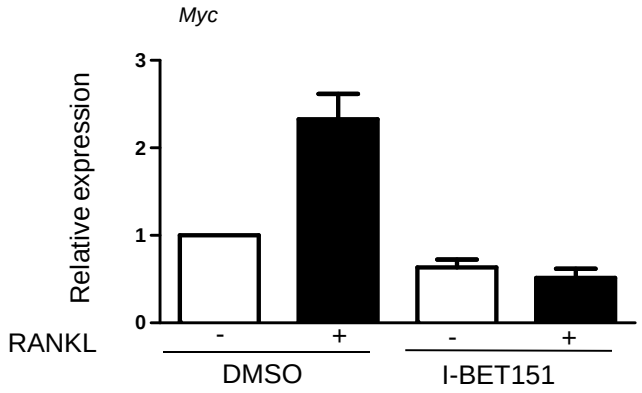

Supplementary Figure 15. I-BET151 suppresses RANKL-induced Myc expression in mouse OCPs. Mouse bone marrow cells from C57BL/6 mice were cultured with M-CSF (20 ng ml^{-1}) for 4 days and then exposed to either DMSO (vehicle control) or I-BET151 (500 nM). After 1hr, RANKL (100 ng ml^{-1}) was added, and cells were cultured with RANKL for two days. *Myc* mRNA was measured using real-time PCR. mRNA levels were normalized to the expression of GAPDH mRNA. Data are shown as means ± SEM from three independent experiments.

Mouse OCPs

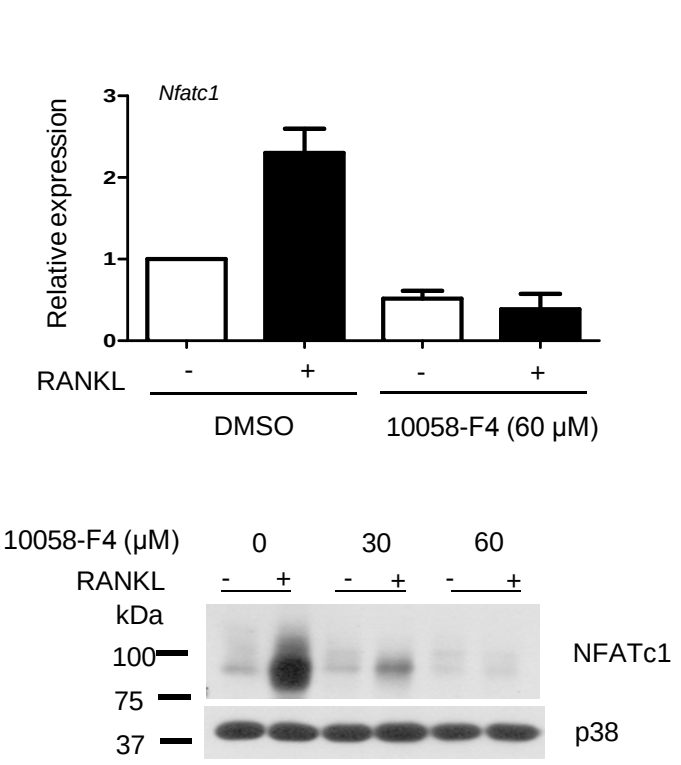

Supplementary Figure 16. A MYC inhibitor, 10058-F4, suppresses RANKL-induced NFATc1 expression in mouse OCPs. Mouse bone marrow cells from C57BL/6 mice were cultured with M-CSF (20 ng ml^{-1}) for 4 days and then exposed to either DMSO (vehicle control) or 10058-F4 at the indicated doses. After 1hr, RANKL (100 ng ml^{-1}) was added, and cells were cultured with RANKL for two days. **a.** *Nfatc1* mRNA was measured using real-time PCR. mRNA levels were normalized to the expression of GAPDH mRNA. **b.** Whole-cell lysates were immunoblotted with NFATc1and p38 antibodies. Images have been cropped for presentation; full size blots are shown in Supplementary Figure 18.

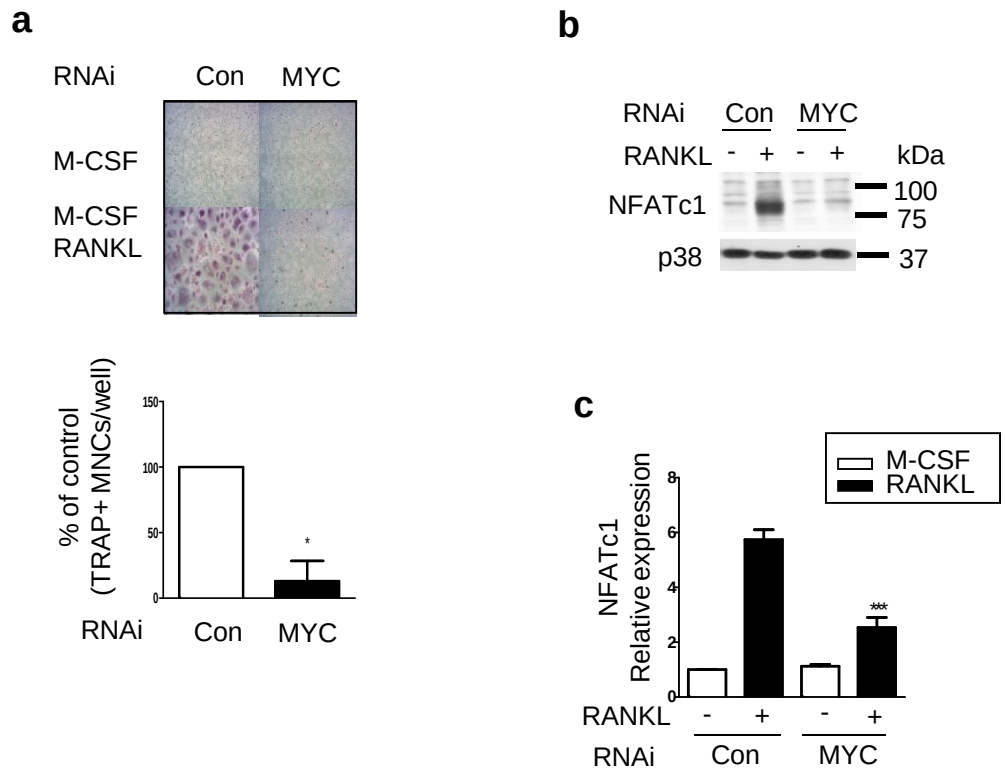

Supplementary Figure 17. MYC plays an important role in osteoclastogenesis. Human monocytes were nucleofected with control or MYC-specific small interfering RNAs (siRNAs). **a.** Osteoclastogenesis assay. TRAP-positive, multinucleated osteoclast formation was visualized by TRAP staining. *Upper panel*, Representative results obtained from one donor are shown. *Lower panel*, Data are shown as mean ± SEM from four independent donors. The number of osteoclasts obtained using control siRNA for each donor is set as 100%. Data are shown as means ± SEM from three independent experiments. * :$P < 0.05$ by One-way ANOVA. **b.** Immunoblot of NFATc1 and p38 expression in human OCPs after 2 days of RANKL treatment. Images have been cropped for presentation; full size blots are shown in Supplementary Figure 18. **c.** NFATc1 mRNA was measured using real-time PCR. mRNA levels were normalized to the expression of GAPDH. , Data are shown as means ± SEM from three independent experiments. *** :$P < 0.001$ by One-way ANOVA.

Fig 4c

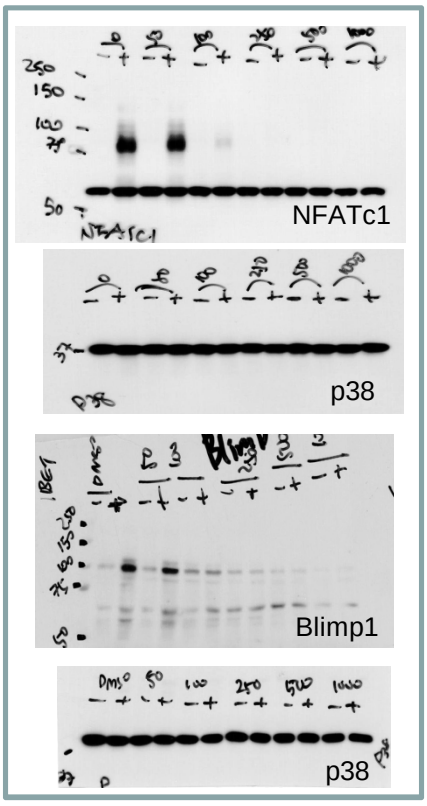

Fig 5c

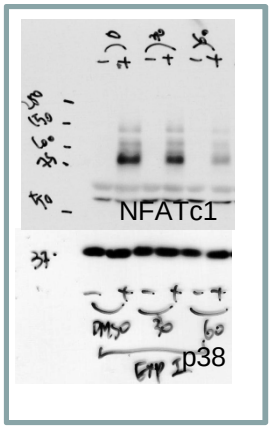

Supplementary Fig .12a

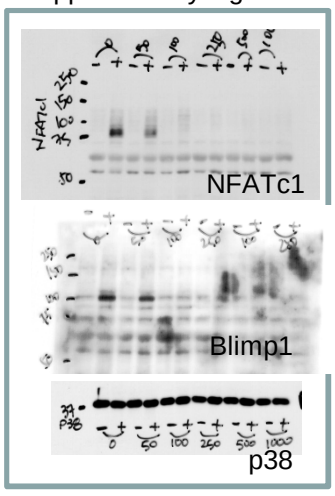

Supplementary Fig .13a

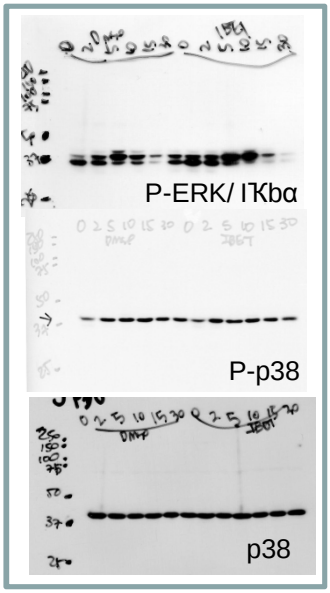

Supplementary Fig .16b

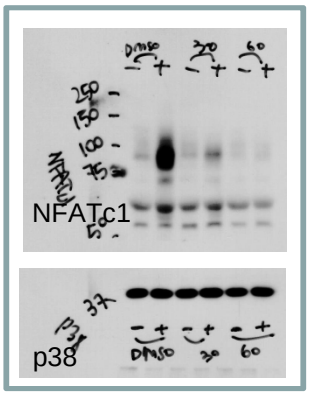

Supplementary Fig .17b

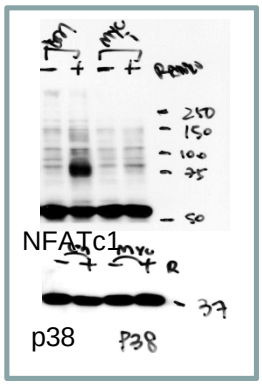

Supplementary Figure 18. Full blot images of the figures and supplementary figures used in this paper. After transferring proteins into the membrane, the membrane is splitted between 50 kDa and 37kDa. Lower part of the membrane is blotted with p38 antibody.

Supplementary Table 1.

Genes were induced by RANKL (>2fold) and inhibited by I-BET (>2 fold): 465 genes

ABCE1
ACAD11
ADAMDEC1
ADAMTS14
ADAMTS2
AEN
AFAP1
AK4
AK8
ALDH1B1
ALG1L
ALKBH2
ALS2CL
ANLN
APOBEC3B
ARHGAP23
ARNT2
ATAD2
ATAD3A
ATAD3B
ATIC
ATP6V0D2
AURKAPS1
AURKB
B4GALT2
BAHCC1
BAMBI
BCAR1
BCL7A
BHLHE40
BIRC5
BOLA3
BOP1
BRCA1
BRIX1
BUB1
BUB1B
BYSL
C10orf2
C11orf82
C12orf23
C14orf34
C16orf59
C17orf53
C1orf198
C1orf21
C1orf226
C1QBP
C7orf74
C9orf140
C9orf30
C9orf41
CA2
CCDC34
CCDC86
CCL24
CCL7
CCNA2
CCNB2
CCND1
CCNE1
CCNE2
CD109
CDC20
CDC25A
CDC42EP1
CDC42EP5
CDC45
CDC6
CDCA3
CDCA5
CDCA7
CDCA8
CDK1
CDT1
CENPA
CENPF
CENPH
CENPI
CENPK
CENPM
CEP55
CHAF1B
CHCHD4
CHEK1
CHPF
CKAP2L
CKB
CKS1B
CLCF1
CLSPN
COL18A1
COL27A1
COL6A2
COQ3
CSPG4
CTPS
CTTN
CXCL5
CYCS
CYP27B1
DCTPP1
DDX21
DEPDC1B
DHODH
DIAPH3
DIXDC1
DLAT
DLEU1
DLGAP5
DMPK
DNA2
DOT1L
DPH2
DPP4
DSCC1
DTL
E2F1
E2F2
E2F8
EBNA1BP2
EFCAB4B
EHD2
EIF2B3
ELOVL6
ENO3
EPT1
ESCO2
ESYT3
EXO1
EXOSC5
EXT1
F2R
F3
F5
FAIM
FAM108C1
FAM109A
FAM111B
FAM134B
FAM19A3
FAM19A4
FAM40B
FAM54A
FAM86C2P
FANCA
FANCI
FARSB
FASN
FEN1
FILIP1L
FJX1
FKBP11
FKBP4
FLNB
FN1
FNBP1L
FOSL1
FOSL2
FOXM1
FUT7
FXN
GAL
GALNT14
GCSH
GINS2
GINS3
GLB1L2
GMPR
GNPNAT1
GOLM1
GPATCH4
GPR125
GREM1
GRPR
GSG2
GTPBP4
GTSE1
GXYLT2
HELLS
HIC1
HJURP
HMMR
HPDL
HSP90AB4P
HSPB1
HSPD1
HSPE1
HSPG2
HSPH1
HTRA3
HYAL1
IARS
IFI27
IFRD2
IGFBP6
IGSF10
IL15RA
IL1R2
IL7R
ILDR1
IMP4
IPO4
ISOC2
ITGA11
ITGB3
ITPR1
JDP2
KANK1
KIAA0020
KIAA0040
KIAA0101
KIAA0664
KIAA1161
KIF11
KIF18B
KIF20A
KIF23
KIF2C
KIFC1
LAPTM4B
LAT
LDHA
LEPREL1
LGALS2
LIF
LOC100128191
LOC100128881
LOC100289511
LOC100506054
LOC729080
LOXL2
LTBP2
LTV1
MAD2L1
MANEAL
MAOA
MARS2
MATK
MCM10
MCM2
MCM3
MCM4
MCM7
MELK
METRN
METTL1
MGST1
MKI67
MLLT11
MMACHC
MND1
MNS1
MPP6
MRGPRF
MRPL1
MRPL12
MRPL24
MRPL3
MRPL4
MRPL46
MRTO4
MT1H
MTFP1
MTHFD1
MTHFD1L
MYBBP1A
MYBL2
MYC
MYEOV
MYO10
MYO19
MYO1B
NAP1L5
NAT14
NAV2
NCAPG
NCAPH
NCS1
NDC80
NDFIP2
NDUFS8
NFATC1
NLE1
NME1
NME1-NME2
NOLC1
NOP16
NOS1AP
NOV
NPM3
NRIP3
NUDT8
NUF2
ODC1
ORC1
ORC6
OXCT1
OXR1
PA2G4
SHANK3
SHCBP1
SHPK
SIGLEC15
SIK1
SIX5
SKA1
SKA3
SLC25A15
SLC25A22
SLC25A23
SLC27A5
SLC2A1
SLC35E4
SLC35F2
SLC35G1
SLC38A5
SLC39A14
SLC39A8
SLC43A3
SLC7A1
SLC9B2
SLCO4A1
SPAG5
SPARC
SPC24
SPC25
SPHK1
SRM
ST18
ST6GALNAC4
STAMBPL1
STEAP1
STEAP3
STIL
STRADB
SULT1B1
SUPT3H
TANC2
TBC1D4
TEX10
TFRC
TGFB3
THOP1
TIMM17A
TIPIN
TK1
TLE1
TMEM158
TMEM237
TMX2
TNFRSF12A
TNFRSF6B
TOMM34
TOMM40
TOP2A
TPX2
TRAK2
TRAP1
TRIP13
TRMT61A
TROAP
TSPAN7
TSR1
TTC4
TTK
TUBA8
TXLNB
TYMS
UBE2C
UBE2T
UCHL1
UHRF1
UNG
USP18
PA2G4P4
PACSIN3
PAICS
PAM16
PAQR5
PDCD1LG2
PDF
PDSS1
PEMT
PFAS
PFKP
PGAM1
PGAM4
PHF17
PHLDA2
PHLDA3
PIGW
PKIA
PKN3
PLEKHF1
PLK1
PLK4
PLS3
PODXL2
POLE2
POLQ
POLR1A
POLR3D
POLR3G
POLR3K
PPARGC1B
PPM1J
PPP1R14B
PPYR1
PRC1
PRIM1
PRKCH
PROCR
PTK2
PTPN22
PTPRF
PVT1
PYCR1
PYCRL
RAB38
RAC3
RAD51
RAD54B
RAI14
RANBP1
RBFA
RBFOX2
RBP5
RECQL4
RFC3
RFX8
RGS16
RMI2
RNF208
RRAD
RRM2
RRP12
RRS1
RUVBL1
S100A2
S100A3
SCFD2
SCG5
SCML2
SDC1
SEMA3A
SFXN1
SFXN4
SGOL1
UST
UTP20
VARS
WDHD1
WDR12
WDR34
WDR4
WDR76
WEE1
WWC1
YRDC
ZDHHC9
ZNF366
ZNF367
ZNF462
ZWINT

Supplementary Table 2

NFATc1 dependent genes among 465 RANKL-induced and I-BET suppressed genes

ITGB3	DPP4
SLC9B2	TMEM158
F2R	CDCA5
RAB38	TTK
EXT1	TK1
SULT1B1	ILDR1
SPHK1	FOSL1
TFRC	PRIM1
PPARGC1B	CENPH
SEMA3A	RNF208
MYO1B	HELLS
TSPAN7	CENPK
FAM134B	MCM3
POLR3K	CDCA7
NRIP3	COL18A1
PLEKHF1	RFC3
SHANK3	DTL
CD109	ELOVL6
IL15RA	EXO1
PRKCH	PTK2
SFXN4	COL6A2
F5	KIF23
HSPG2	TPX2
RGS16	HSPH1
TYMS	POLE2
LGALS2	BUB1
RAI14	SGOL1
FN1	MCM4
RBFOX2	SHCBP1
HTRA3	DNA2
OXR1	TIPIN
LIF	ANLN
OXCT1	SPAG5
FJX1	MLLT11
FOSL2	CCND1
ENO3	BYSL
ST6GALNAC4	KIF2C
MRPL3	TRIP13
CKB	CEP55
POLR1A	UHRF1
NOV	RRAD
BCAR1	MCM7
GMPR	GRPR
NDUFS8	MRPL1
CSPG4	HMMR
CCL7	TGFB3
WWC1	MCM2
SIX5	UBE2C
TXLNB	MPP6
CHEK1	FANCI
MTHFD1	SCML2
SKA1	SPC25
CDC6	NCAPG
MND1	PLK4
IL7R	MYC
FANCA	MKI67
CDC20	KIF11
CCNE2	SPARC
RAD51	PRC1
BRCA1	
MELK	

Supplementary Table 3

A list of primers used in this study:

Gene Symbol	Sequence
NFATC1	CTTCTTCCAGTATTCCACCTAT TTGCCCTAATTACCTGTTGAAG
MYC	GTGCATCGACCCCTCGGTGG TTGCGAGGCGCAGGACTTGG
BCL6	CCTCGCCAGCCACAAGACCG CTGGCTCCGCAGGTTTCGCA
IRF8	TGCGCTCCAAACTCATTCTCGTG GTCTGGCGGCGGCTCCTC
MAFB	CTCAGCACTCCGTGTAGCTC GTAGTTGCTCGCCATCCAGT
CTSK	CTCTTCCATTTCTTCCACGAT ACA CCA ACT CCC TTC CAA AG
ITGB3	GGAAGAACGCGCCAGAGCAAAATG CCCCAAATCCCTCCCCACAAATAC
Nfatc1	CCCGTCACATTCTGGTCCAT CAAGTAACCGTGTAGCTCCACAA
Myc	GCCGATCAGCTGGAGATGA GTCGTCAGGATCGCAGATGAAG
Ctsk	AAGATATTGGTGGCTTTGG ATCGCTGCGTCCCTCT
Itgb3	CCGGGGGACTTAATGAGACCACTT ACGCCCCAAATCCCACCCATACA
Cxcl1	GGTGTCCCCAAGTAACGGAG TTGTCAGAAGCCAGCGTTCA
Cxcl2	TGCAGTCGGATGGCTTTCAT GCACTGTGCCTTACGAGGAA
Il1b	CAACCAACAAGTGATATTCTCCATG GATCCACACTCTCCAGCTGCA

NFATC1 promoter	CCAGTGAAGCGCTTTTCCAA CCGGCATGCTGAAGTCATTA

Supplementary Methods

Analysis of bone phenotype. To measure bone mineralization in the OVX model, mice were intraperitoneally injected with Calcein (green) at 10 μg g^{-1} (body weight) twice, 7 days apart. Two days after the second injection, femurs were collected, fixed in 80% ethanol, embedded in poly(methyl methacrylate) as described previously [1], and then cut into 8–10 μm sections. Histomorphometry analysis using OsteoII software (Bioquant, Nashville, TN) was performed on trabecular bone within the femoral metaphysis. Mineral apposition rate (MAR) was determined by measuring the distance between two fluorochrome-labeled mineralization fronts. The mineralizing surface was determined by measuring the double labeled surface and one-half of single labeled surface, and by then expressing this value as a percentage of total bone surface. The Bone Formation Rate (BFR) was then expressed as MAR x mineralizing surface/total bone surface, using a surface referent.

Osteoblast differentiation analysis. Primary osteoblast precursors were isolated from calvaria of wild type mice by using the digestion solution containing type I collagenase and dispase II (Invitrogen). Cells were cultured with α-MEM containing 10% FBS, 50 μg/ml of ascorbic acid, and 8 mM beta-glycerophosphate. For osteoblast marker gene expression, total mRNA was purified from osteoblast cultures at day 10. Osteoblasts were stained with Alizarin Red after 21 days of culture and Alizarin Red staining was quantified by colorimetric analysis at OD_{405}.

Supplementary References

1. Erben, R.G. Embedding of bone samples in methylmethacrylate: an improved method suitable for bone histomorphometry, histochemistry, and immunohistochemistry. *J Histochem Cytochem* **45**, 307-313 (1997).

2. Charles, J.F., *et al.* The collection of NFATc1-dependent transcripts in the osteoclast includes numerous genes non-essential to physiologic bone resorption. *Bone* **51**, 902-912 (2012).